Available online at www.sciencedirect.com
ScienceDirect
Intermetallics 16 (2008) 508–517
Intermetallics
www.elsevier.com/locate/intermet

# Hydrogen diffusion in $Mg_2NiH_4$ intermetallic compound

Jiří Čermák*, Lubomír Král, Bohumil David

*Institute of Physics of Materials, AS CR v. v. i., Žižkova 22, CZ-616 62 Brno, Czech Republic*

Received 20 September 2007; received in revised form 6 December 2007; accepted 18 December 2007
Available online 15 February 2008

**Abstract**

Coefficients of hydrogen diffusion in $Mg_2NiH_4$ were measured by a volumetric method at temperatures ranging from 449 to 576 K. Experimental material was prepared in two ways: by melting and casting, and by ball-milling and compacting into pellets. Hydrogen charging was performed from the hydrogen gas phase at elevated pressure and temperature. Pellets were charged in two different modes, resulting in structures with either a high fraction of twinned low-temperature phase LT2 or a low fraction of LT2. It was observed that LT2 considerably slowed down the hydrogen desorption rate. Activation enthalpy of hydrogen diffusion in high-temperature phase (above transition temperature $T_{tr} \sim 508$ K) is approximately half of the value obtained for the low-temperature region. Coefficients of hydrogen diffusion in low-temperature un-twinned phase LT1 are by a multiplication factor of about 20 higher than those of the twinned phase LT2.


*Keywords:* A. Intermetallics, miscellaneous; B. Diffusion; B. Hydrogen storage; B. Phase transformations; D. Microstructure

## 1. Introduction

Hydrogen is a very prospective fuel for both direct combustion and in electrochemical batteries and fuel cells, with nuclear fusion constituting a very special branch in itself. There is a wide range of issues that are intensively studied, ranging from environmental friendliness of hydrogen production itself to special materials for new hydrogen technologies.

One of the issues of utmost importance is hydrogen storage in solid media. There is a wide variety of materials considered for hydrogen storage materials (HSMs); for an overview see e.g. Refs. [1–3]. It is worth noting that in some materials the stored hydrogen density is even higher than the liquid hydrogen density [4]. The main issues to be solved in this sphere include sufficient storage capacity, high-cycle durability, resistance to contaminant gases, and sufficient rate of hydrogen charging/decharging (C/D) under moderate conditions (not too high temperature and pressure).

Magnesium-based alloys rank among the most frequently studied HSMs for two main reasons: first, magnesium is a very cheap element abundant on the Earth and second, light Mg-based matrix has provided the best weight-storage ratio so far. However, pure Mg is not a suitable HSM due to the poor kinetics of the C/D cycle. Therefore, it is alloyed with other elements, frequently with nickel. In particular, eutectic mixtures (Mg)/$Mg_2Ni$ and pure $Mg_2Ni$ intermetallic compound are of interest as base materials. Although the other intermetallic compound $MgNi_2$ in the Mg–Ni binary system [5] shows a certain solubility of hydrogen [6], it is commonly not considered a prospective HSM at present.

Even alloyed, Mg-based HSMs need temperatures about 470 K for C/D, which makes them unsuitable as energy sources in personal and household appliances. Therefore, there is a considerable and constant effort to lower the stability of Mg-based hydrides and, at the same time, to preserve their favorable storage capacity – see e.g. in Refs. [7–11].

Even though there are some studies on C/D kinetics applicable to Mg-based alloys [12–20], only the rate constants are known. The theory of the C/D kinetics is often based on Johnson–Mehl–Avrami model – see e.g. in Ref. [21]. Contrary to the conclusion often drawn, namely that the process of desorption is controlled by diffusion [12,13,16,21], quantitative data describing hydrogen diffusion itself are very sparse in

* Corresponding author. Tel.: +420 532 290 422; fax: +420 541 218 657.
*E-mail address:* cermak@ipm.cz (J. Čermák).

0966-9795/$ - see front matter © 2007 Elsevier Ltd. All rights reserved.
doi:10.1016/j.intermet.2007.12.010

the literature. In Ref. [15], the authors declare the α/β interphase motion at high temperatures (α – solid solution of hydrogen in matrix, β – hydride), nucleation-and-growth at ''early stages'' and diffusion at ''later stages'' as respective controlling mechanisms. In Refs. [16,18], the authors tested a number of known rate equations and chose ''the best one'' for their materials studied. It should be noted, however, that the choice of the optimum equation (and the probable kinetic mechanism governing the respective phase change) is very difficult in this way.

It is known that the phase $Mg_2NiH_4$ compound undergoes phase changes between the room temperature and the melting point, which complicates the kinetic study of the C/D processes in the material. The history of phase analysis in $Mg_2NiH_4$ dates back to 1979 when Gavra and Mintz [22] identified the cubic high-temperature phase above $T_{tr} = 508$ K. In 1980s, a series of studies appeared – see e.g. in Ref. [23–32], which can be summarized as follows: the high-temperature (HT) phase is fcc cubic, derived from $CaF_2$-type structure. Magnesium ions form a cube around $[Ni^0H_4]$ complex ($Ni^0$ – effectively zero-valent Ni atom; H atoms occupy six of eight vertexes of octahedral centering in Ni atom), building an anti-fluorite structure (anions occupy the fcc lattice points, complexes reside in four tetrahedral sites). The exact location of the hydrogen atoms around Ni center can be specified only approximately. It is possible to say [30] that the H atoms are located at a sphere with a radius 1.5 Å. Slightly more detailed information on the H location can be found in Ref. [33]: a square planar order of the H atoms in the complex implies metallic properties, whereas regular tetrahedron results in a semiconductor-like character of the compound (for step-like changes of electric conductivity – see also in Ref. [30]). Upon cooling-down, the HT transforms into a monoclinically distorted low-temperature (LT) phase with slightly distorted tetrahedral $[Ni^0H_4]$ complex. LT exists in two modifications – un-twinned (LT1) and microtwinned (LT2). Microtwinning occurs on the basic cell level. The ratio of LT1/LT2 depends sensitively on the thermo-mechanical history of the sample and influences, to a certain extent, the electrical conductivity and the color of the LT [30]. The presence of LT2 may be indicated by typical peak in the XRD diffraction profile at $2\theta = 23.7^\circ$ (with Cr Kα1 radiation) [25,30,31].

The aim of the present study is to obtain diffusion coefficients of hydrogen in $Mg_2NiH_4$ intermetallic compound for both HT and LT temperature regions. The coefficients allow to quantify the rate of hydrogen diffusion-controlled processes occurring in the compound.

## 2. Experimental

### 2.1. Preparation of experimental materials

The intermetallic compound $Mg_2Ni$ was prepared from pure components 3N6 Ni and 3N8 Mg. Splinters of pure components were ball-milled in air using *Fritsch-Pulverisette6*. The ratio of the components was Mg–54.5 wt.% Ni. The thickness of the splinters was about 0.1 mm and the milling conditions were as follows: mass ratio of balls to that of the milled mixture $r = 25$ and milling time regime: 10 min milling + 50 min relaxation – repeated 20 times. The milled powder was compacted into pellets of a diameter of 20 mm × 5 mm in height.

The cast modification of the compound was prepared by induction melting of the pellets in the MgO crucible under Ar protective atmosphere. The ingot was cut into slices about 2 mm thick and ground down with metallographic papers to foils of a final thickness of 1.5 mm.

### 2.2. Hydrogen charging

Hydrogenation followed immediately after preparation of the pellets/foils by isothermal annealing in a pressure vessel. Pressure of pure (5N3) hydrogen was 30 bar and the charging temperatures $T_c$ were 423 and 673 K. The charging time was several hours for pellets and 14 days for foils. In all cases, almost complete charging was achieved since no further significant increase in hydrogen content in the samples was observed after additional anneal, which was monitored by precise weighing.

### 2.3. SEM observation

#### 2.3.1. Pellets

The sample structure (see Fig. 1) was checked by SEM JEOL JSM 6460 equipped with EDAX/WEDAX Oxford Instruments analyzer. As is shown in Fig. 1a, the compacted pellets were porous and consisted of compact grains of a mean size of about 20 μm. The chemical composition of the grains coincided with the stoichiometry of $Mg_2Ni$ compound.

The mean grain size of hydrogen charged $Mg_2Ni$ samples was slightly reduced due to fragmentation of the largest grains. As is shown in Fig. 1b, the surface of the grains after hydrogen desorption was covered with small particles (of ca. 2 μm in diameter) of desorbed α phase (i.e. $Mg_2NiH_x$; $x = 0–0.3$).

#### 2.3.2. Foils

The structure of the cast material is shown in Fig. 2. Due to incongruent solidification [5], there are three components present. The first, the $MgNi_2$ compound, precipitates forming agglomerates of rectangular crystallites in the melt – see the light rectangular particles in Fig. 2a. This phase participates in the hydrogen C/D process in a negligible extent only [6]. Below 1033 K, $Mg_2Ni$ starts to precipitate and the rest of Mg-enriched melt solidifies between the grains of grown $Mg_2Ni$ as a fine eutectic.

During hydrogen charging, the grains transform to $Mg_2NiH_4$ and $MgH_2$ is nucleated in the eutectic. The latter phase grows forming rows of individual crystallites decorating the grain boundaries – see Fig. 2b. Progressive hydrogen charging brings about an increase in the internal stress and de-cohesion of the material (Fig. 2c).

### 2.4. XRD phase analysis

X-ray profiles were obtained by X'Pert Pro MPD device (PANanalytical B.V., Almelo, the Netherlands) using Co Kα

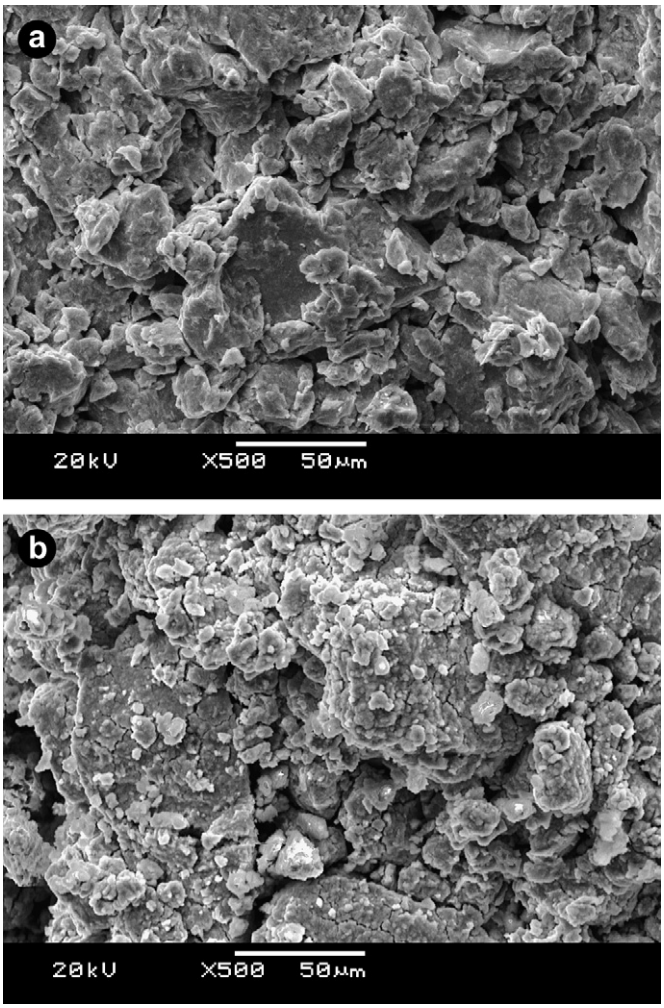


Fig. 1. Structure of compacted pellets of $Mg_2Ni$ intermetallic. Before hydrogen charging (a) and after decharging (b).

radiation and interpreted by means of the HighScore Plus software with commercial databases [34–36].

The results can be illustrated by the most significant reflexions marked in XRD pattern shown in Fig. 3. It is clear that the prevailing phase in the charged samples was $Mg_2NiH_4$. In the cast sample (Fig. 3a) and in the pellets charged at a low temperature below the $T_{tr}$ (Fig. 3c), $MgH_2$ phase and a certain amount of $Mg_2NiH_{0.3}$ also were present. No traces of magnesium oxide and magnesium hydroxides were detected in the experimental samples.

It is interesting to compare the amount of the twinned LT2 phase (typical line at $2\theta = 27.3^\circ$ [25,29–31]) in the charged samples. Whereas the pellets charged above $T_{tr}$ (Fig. 3b) contain a considerable amount of twinned LT2 phase, in the cast sample charged above $T_{tr}$ (Fig. 3a) and in the pellets charged below $T_{tr}$ (Fig. 3c), the LT1 phase prevail.

In the desorbed samples, only the $\alpha$ phase ($Mg_2NiH_x$; $x = 0–0.3$) is present, which is shown in Fig. 3d.

### 2.5. DSC measurements

The aim of a DSC measurement was to assess contributions of the two hydrides $Mg_2NiH_4$ and $MgH_2$ to total hydrogen

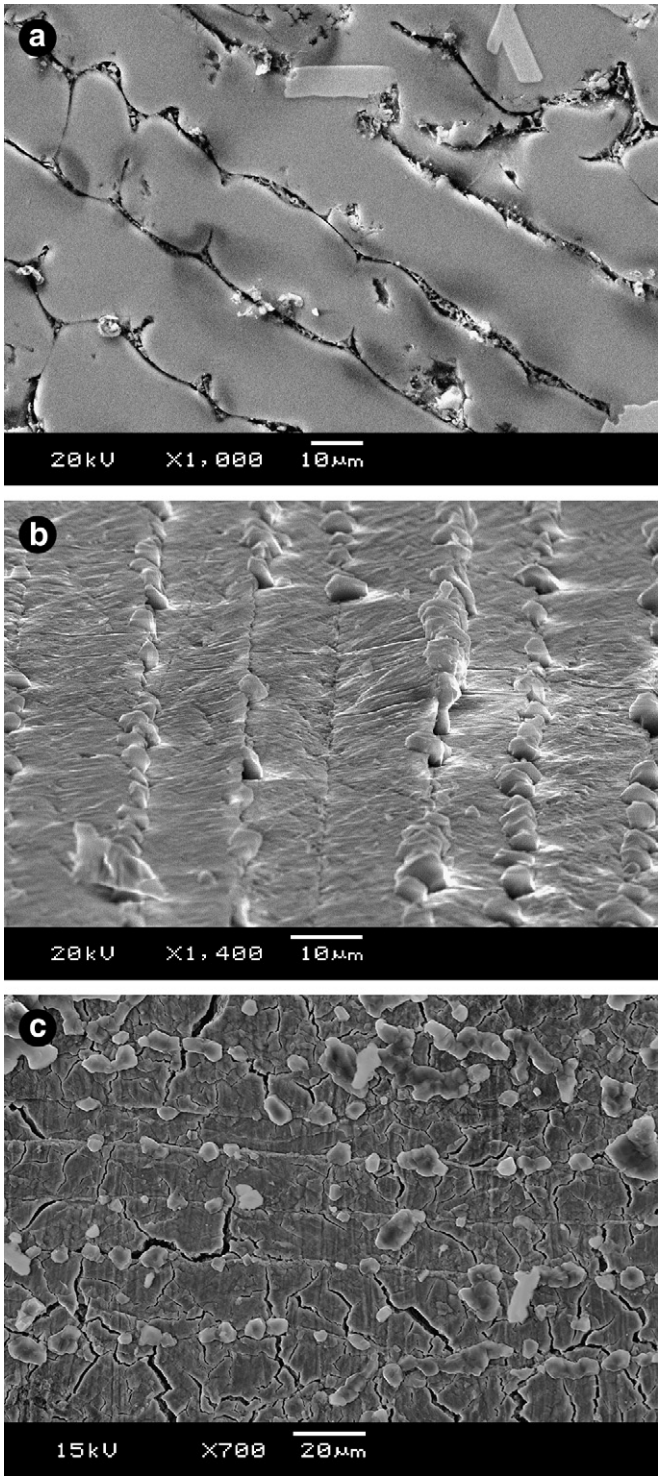


Fig. 2. SEM micrograph of cast $Mg_2Ni$ intermetallic. Before hydrogen charging (a): grain interior – $Mg_2Ni$, light rectangular particles – $MgNi_2$, fine eutectic (Mg)/$Mg_2Ni$ at grain boundaries; free surface after hydrogen charging (b): rows of $MgH_2$ particles grown at grain boundaries; after hydrogen decharging (c): $Mg_2NiH_4$ fragmented grains transformed to $Mg_2NiH_{0-0.3}$, $MgH_2$ particles remained unchanged.

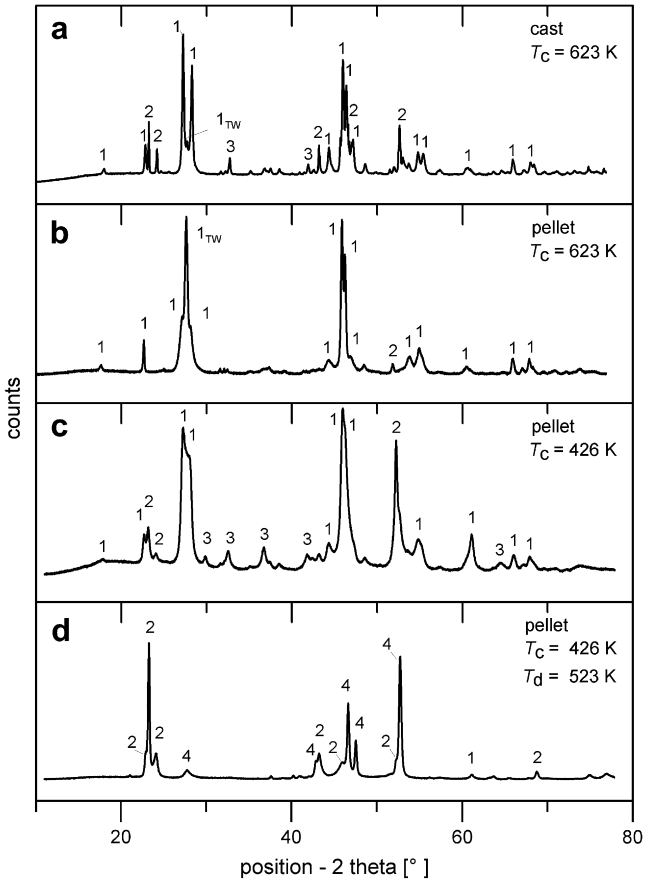


Fig. 3. XRD pattern of samples. 1 – $Mg_2NiH_4$ (LT1 – un-twinned), $1_{TW}$ – (LT2 – twinned), 2 – $Mg_2NiH_{0.3}$, 3 – $MgH_2$, 4 – $Mg_2Ni$. $T_c$ – charging temperature, $T_d$ – decharging temperature.

desorption (identified by significant endothermic reactions) at various desorption temperatures.

The DSC measurements were done using differential scanning calorimeter Netzsch DSC 204 F1 from room temperature up to 773 K. The DSC spectra were taken during the temperature increase only at the constant rate of 10 K/min.

It is obvious from Fig. 4 that $Mg_2NiH_4$ releases hydrogen mostly at two temperatures: the lower is close to transformation temperature $T_{tr}$ between the LT and the HT phases (518 K according to Ref. [37] or 508 K according to Ref. [23]), which is, at the same time, close to temperature $T_{eq} = 517$ K calculated from van't Hoff's equation [38] for $p_{eq} = 1$ bar (i.e. for the pressure of DSC measurements). The remaining hydrogen is released at a higher temperature close to 600 K.

The results of the DSC measurements showed that hydrogen released at temperatures below 576 K (maximum desorption temperature used in the present work for measurement of hydrogen diffusion coefficient) came exclusively from the $Mg_2NiH_4$ hydride phase.

### 2.6. Mass spectroscopy analysis of the desorbed gaseous phase

A semi-quantitative analysis of the gaseous phase desorbed from the studied samples was carried out at the Masaryk

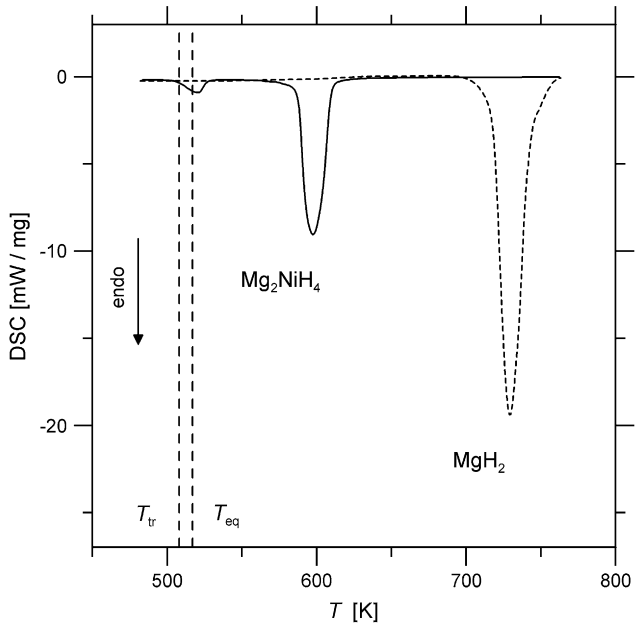


Fig. 4. DSC curves of experimental material measured at the rate of 10 K/min. $T_{tr}$ – transformation temperature between HT and LT, $T_{eq}$ – equilibrium temperature of $Mg_2NiH_4$ calculated from van't Hoff equation [38] for $p = 1$ bar. $MgH_2$ – particles extracted from the surface layer of the cast $Mg_2NiH_4$ sample.

University of Brno, Czech Republic, using quadrupole mass spectrometer TRIO 1000 Fisons Instrument, Finnigan MAT.

Negligibly small traces of residual air were detected in mass channels 28 ($N_2$), 32 ($O_2$) and weak traces in channels 18 ($H_2O$), 40 (Ar) and 44 ($CO_2$) by scanning analysis (dependence of signal intensity on the temperature in temperature interval from room temperature to 673 K). Hence, the gaseous phase released between the room temperature and 673 K should be identified exclusively with hydrogen (which could not be directly detected by this method).

### 2.7. Hydrogen desorption

We carried out the desorption experiments in a vacuum chamber of a calibrated volume, allowing to heat the sample isothermally at selected temperatures $T_d$ and to measure the time dependence of desorbed hydrogen pressure $p(t)$. The thermocouple Pt/PtRh was in contact with the sample, the typical mass of which was 3 g.

## 3. Results and discussion

### 3.1. Desorption curves

The measurement of desorption curves $p = p(t)$ was done in isothermal regime since the temperature increase of the sample (after being inserted into a tempered furnace) was negligibly short, compared to the time of decharging. All of the measured desorption curves are plotted in Figs. 5–7 in coordinates relative pressure $r = (p - p_s)/(p_f - p_s)$ vs time $t$. The starting pressure $p_s$ was always 2 mbar and the maximum

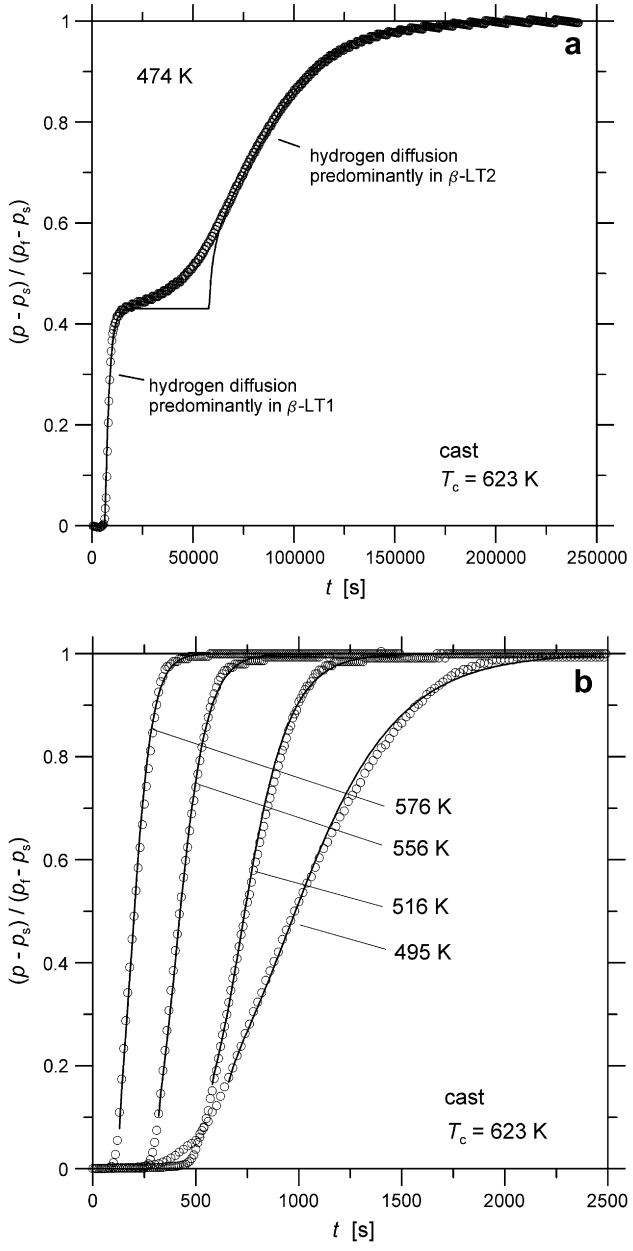


Fig. 5. Desorption curves measured with cast $Mg_2NiH_4$ samples charged at $T_c = 623$ K and desorbed at $T_d = 474$ K (a) and $T_d = 495–576$ K (b). Full lines – Eqs. (1)–(4).

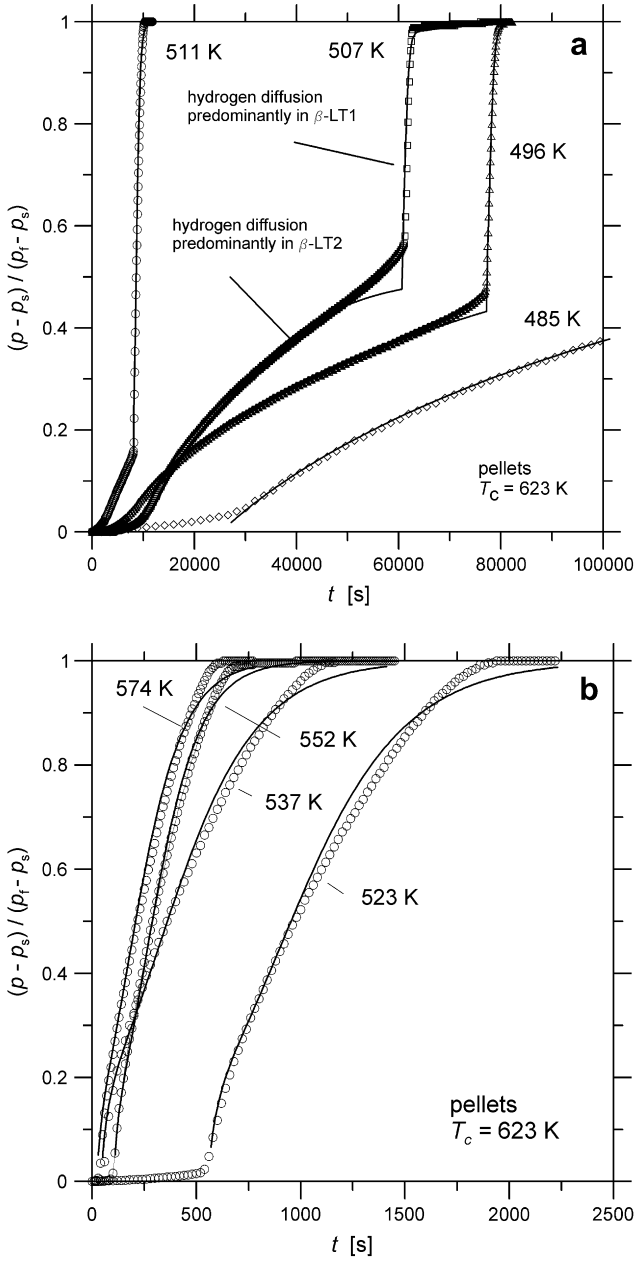


Fig. 6. Desorption curves measured with pellets $Mg_2NiH_4$ charged at $T_c = 623$ K and desorbed at $T_d = 485–511$ K (a) and $T_d = 523–574$ K (b). Full lines – Eqs. (1)–(4).

pressure $p_f$ reached during the desorption ranged from 80 to 200 mbar.

It is obvious that the character of the curves changed close to the HT/LT transformation temperature $T_{tr} = 508$ K. At higher temperatures (Figs. 5b, 6b and 7b), the curves consisted of one branch, whereas below the $T_{tr}$, two more or less distinguishable branches were observed (Figs. 5a, 6a and 7a). However, for pellets charged below $T_{tr}$, the branching of the curves was not so evident (Fig. 7a).

To find out why two branches were observed below $T_{tr}$, a series of several anneals with subsequent XRD measurements were done. The results are shown in Fig. 8. The observation was carried out in seven stages indicated with arrows in Fig. 8a. In Fig. 8b and c, two most instructive parts of X-ray spectra are shown. It was easy to conclude that the *slow* branch appeared, when the LT2 phase prevailed. The phase composition during this stage changed considerably, but it was always dominated by LT2.

The *fast* branch either appeared in a situation where the LT phase contained little or no LT2 component. The breakpoint between the branches occurred when the α phase ($Mg_2NiH_{0.3}$) was nucleated – compare XRD patterns at stages (iv) and (v), especially in position close to $2\theta = 27.5°$ and $2\theta = 46.5°$. The phase composition during the time when the *fast* branch was observed was more or less unchanged (cf. XRD pattern at stages (v) through (vii)). It contained $Mg_2NiH_{0.3}$ and LT1

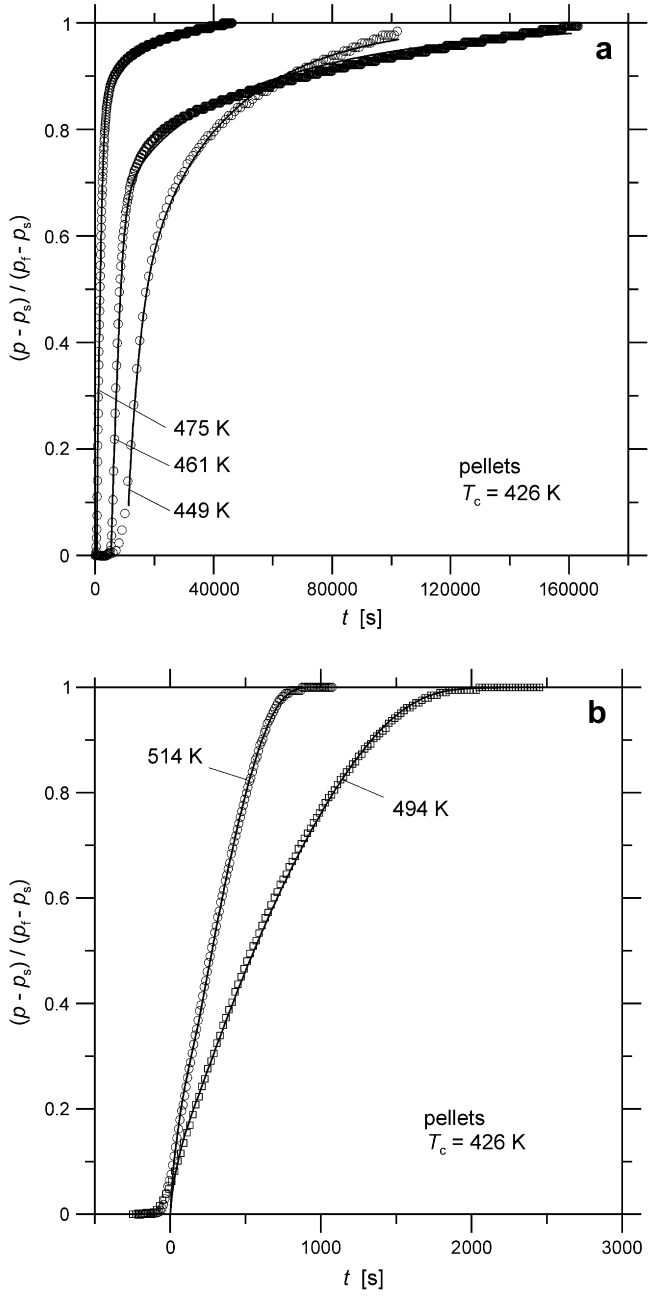


Fig. 7. Desorption curves measured with pellets $Mg_2NiH_4$ charged at $T_c = 426$ K and desorbed at $T_d = 449–475$ K (a) and $T_d = 494$ and 514 K (b). Full lines – Eqs. (1)–(4).

phases. The latter one prevailed especially in samples where LT2 was not present in the initial state (see e.g. Fig. 3a), and the *fast* branch was observed first (Fig. 5a).

It is also worth mentioning a slight shift of peaks No. 2 and 4 related to α phase $Mg_2NiH_{0–0.3}$ towards higher values of $2\theta$ during the desorption (cf. XRD pattern at stages (v) through (vii)). It was caused by reducing of the mean lattice parameter due to hydrogen desorption.

The time sequence of branches (dominance of the *slow* diffusion, followed by the *fast* one as shown in Fig. 6a or a reverse situation shown in Fig. 5a) was determined by the ratio of LT1 and LT2 amounts present in the sample at the beginning of the desorption experiment.

### 3.2. Evaluation of diffusion coefficients

The present experiments with $Mg_2NiH_4$ were carried out under pressures $p$ lying well below the equilibrium pressure $p_{eq}$ calculated for each desorption temperature from the van't Hoff equation [38]. This assured a release of mobile hydrogen atoms in the whole volume of the hydride (homogeneous nucleation of α phase: $\beta \rightarrow \alpha + H$). Under such conditions, the hydrogen evolution from the samples can be described by equations derived for diffusion from the bulk of spatially limited bodies into the finite volume.

It is obvious from Figs. 1a, b and 2c that both charged pellets and fragmented castings are porous agglomerates of small particles that can be quite reasonably approximated by spheres. Therefore, for the relative amount of hydrogen desorbed from the sample into the limited volume, $r = (p - p_s)/(p_f - p_s)$, equations derived in Ref. [39,40] for desorption from the sphere of radius $\rho$ into "well stirred" finite volume can be written down as follows:

$$r = 1 - A\sum_{n=1}^{\infty}\frac{1}{n^2}\int_0^t G(\tau)\exp\left[-\frac{D\pi^2}{\rho^2}n^2(t-\tau)\right]\mathrm{d}\tau, \qquad (1)$$

where $A$ is a constant, $D$ is hydrogen diffusion coefficient and function $G$ describes the rate of hydrogen evolution. The convolution in Eq. (1) reflects the fact that all hydrogen atoms are not free for diffusion at $t = 0$. Integral of $G$ in the interval $t \in (0, \infty)$ should be finite. We suggest the following representation of $G$:

$$G(\tau) = \begin{cases} \delta(0) & (2) \\ \tau_0 \exp\left(-\dfrac{\tau}{\tau_0}\right) & (3) \end{cases}$$

Eq. (2), where $\delta(0)$ is Dirac's delta function in $\tau = 0$, results in the situation known as *instantaneous diffusion source* [40]. It means that all hydrogen atoms in the volume of the particle are free for diffusion at $t = 0$. Eq. (3) with great $\tau_0$ approaches the so-called *constant source* [40], i.e. continuous generation of mobile hydrogen atoms, and medium values of $\tau_0$ allow for initial generation of mobile hydrogen atoms, which fades out with increasing time $\tau$.

The desorption curves with two branches were fitted to linear combination of two terms formally identical to that in Eq. (1):

$$r(t) = f_1 r_1(D_1, t_{01}, A_1, \tau_{01}) + (1 - f_1) r_2(D_2, t_{02}, A_2, \tau_{02}), \qquad (4)$$

where $f_1$ is relative fraction of the first component in the sum (i.e. to the mean relative amount of respective phase and to the mean hydrogen concentration in it) and $t_{01}$, $t_{02}$ are times of onset of the respective branch. The $i$-th term $r_i$ in Eq. (4) is zero

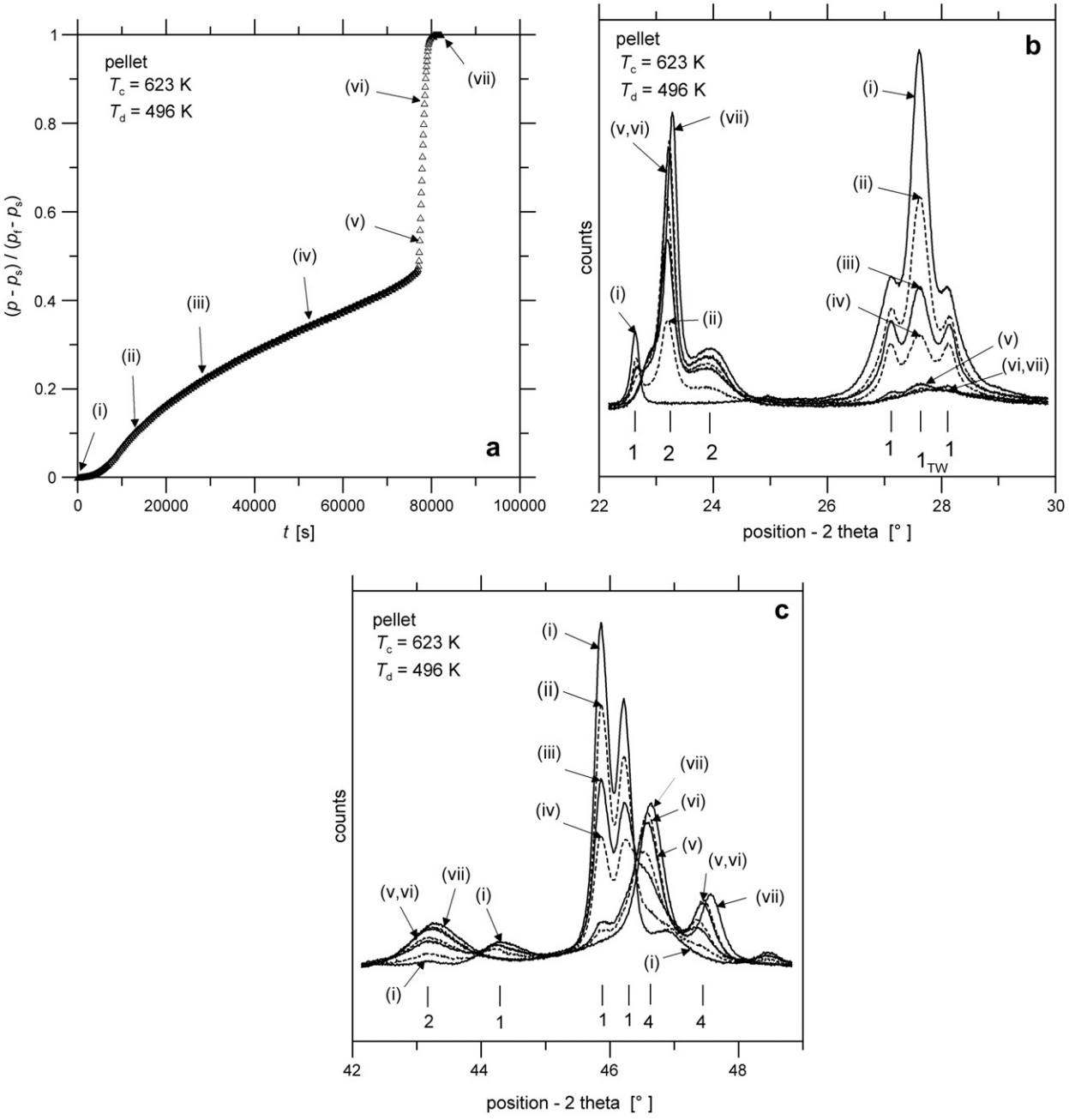


Fig. 8. XRD pattern (Co Kα) measured at stages (i–vii) documenting the time evolution of phase composition in sample with a great content of LT2. Peak labelling is the same as in Fig. 3.

for $t_i = t - t_{0i} < 0$. Diffusion coefficients $D_1$, $D_2$ and parameters $\tau_{01}$, $\tau_{02}$ obtained as fitting parameters, are listed in Table 1. It is worth noting that values of $D_1$ and $D_2$ do not depend significantly on the sequence of desorption branches.

### 3.3. Temperature dependence of D and $\tau_0$

Temperature dependence of diffusion coefficients is shown in Fig. 9. One can see that the transition temperature $T_{tr}$ ($T_{tr} = 518$ K according to Ref. [38] or $T_{tr} = 508$ K [23]) between the HT and LT phases divides the set of the data distinctly: above the $T_{tr}$, one branch produced one effective diffusion coefficient characterizing the hydrogen diffusion in a phase mixture dominated by HT β-phase ($Mg_2NiH_4$). Below $T_{tr}$, two more or less distinct branches resulted in two diffusion coefficients, $D_1$ and $D_2$. Both of them characterize effective hydrogen diffusion in a mixture of phases: the higher one, $D_1$, describes diffusion in mixtures with LT1 phase, the presence of which is a determining factor of the overall, macroscopically observable rate of diffusion process. The lower one, $D_2$, is its counterpart for a mixture of phases containing LT2.

The accuracy of the values of $D$ is given, in particular, by fitting errors that are determined by the adequacy of the

Table 1
Hydrogen diffusion coefficients in $Mg_2NiH_4$ and values of $\tau$ obtained by optimization of Eqs. (1)–(4)

| Material | $T_d$ (K) | LT1, HT | | LT2 | |
|---|---|---|---|---|---|
| | | $D_1$ ($10^{-14}$ m$^2$/s) | $\tau_{01}$ (s) | $D_2$ ($10^{-16}$ m$^2$/s) | $\tau_{02}$ (s) |
| Cast: $T_c = 623$ K, $\rho = 7$ μm | 474 | 0.152 | 1.1 | 2.93 | 20 |
| | 495 | 2.16 | 0.22 | | |
| | 516 | 4.72 | 0.091 | | |
| | 556 | 7.70 | 0.059 | | |
| | 576 | 11.4 | 0.040 | | |
| Pellets: $T_c = 623$ K, $\rho = 10$ μm | 485 | | | 1.12 | 455 |
| | 496 | 2.90 | 0.37 | 3.13 | 63 |
| | 507 | 3.24 | 0.37 | 11.2 | 11 |
| | 511 | 3.57 | 0.26 | | |
| | 523 | 4.47 | 0.25 | | |
| | 537 | 5.59 | 0.20 | | |
| | 552 | 10.1 | 0.11 | | |
| | 574 | 10.2 | 0.11 | | |
| Pellets: $T_c = 426$ K, $\rho = 5$ μm | 449 | 0.127 | 2.9 | 0.759 | 4000 |
| | 461 | 0.225 | 1.1 | 0.431 | 2200 |
| | 475 | 0.405 | 0.71 | 1.52 | 1000 |
| | 494 | 1.20 | 0.19 | | |
| | 514 | 2.74 | 0.087 | | |

$2\rho$ – Mean size of particles or fragments.

physical model. The simple model used for data evaluation assumes a constant diffusion coefficient, but the time variance of phase composition during the desorption (see the sequence of XRD patterns in Fig. 8) suggests that the effective diffusion coefficient may vary. The poor fit in Fig. 6b may be explained by omitting the variance of $D$.

Another major factor influencing the reliability of the obtained values of $D$ is the mean size of the particles/fragments, $2\rho$. As shown in Figs. 1a, b and 2c, the structure is not composed of equally sized particles (or fragments). Even a careful measurement of the mean particle size cannot prevent the influence of early desorption from smaller particles at the beginning of the experiment and the desorption *tail* at long times due to desorption from bigger particles. Hence, any particle size distribution leads to a virtually smaller value of $D$. Considering both principal sources of errors, the typical experimental error was estimated and shown in Fig. 9 as an abscissa.

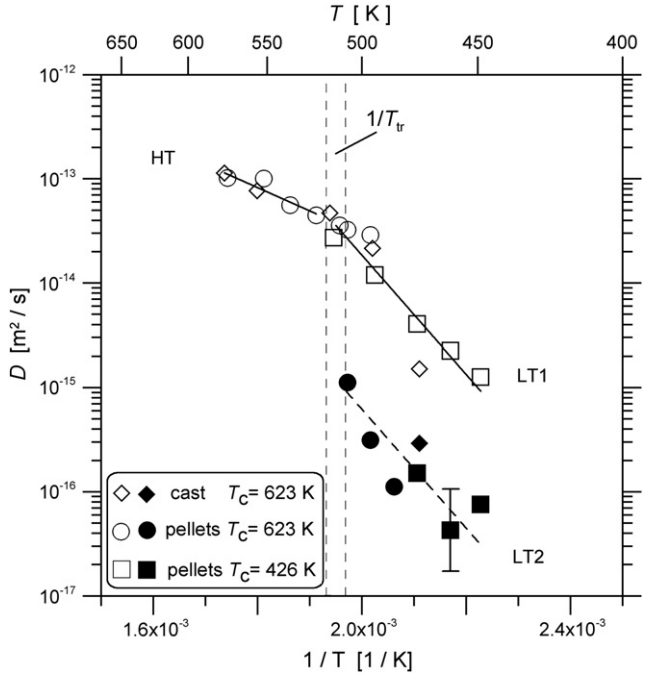


Fig. 9. Arrhenius diagram of hydrogen diffusion coefficients in $Mg_2NiH_4$.

The calculated values of $D$ were fitted to Arrhenius equation $D = D_0 \exp(-Q/RT)$ ($R$ is the gas constant) and frequency factor $D_0$ and activation enthalpy $Q$ were evaluated for all three cases (HT, LT1 and LT2). Let us just remark that – due to large scatter of $D_2$ – the activation enthalpies $Q$ for LT1 and LT2 were set to be equal. The results are summarized in Table 2. The obtained values of $Q$ were confirmed by the cross-cut analysis [41], which gave values $Q = (53.4 \pm 9.3)$ kJ/mol and $Q = (117 \pm 16)$ kJ/mol for HT ($r = 0.5$–$0.9$) and for LT2 ($r = 0.1$), respectively.

In Fig. 10, the present results are compared with literature values. Known values of hydrogen diffusion coefficients in $Mg_2Ni$-H are scattered considerably. Nevertheless, it can be stated that the present results for HT and LT1 fall reasonably between the extrapolated values reported by Group of Senegas et al. [37,42]. However, it is to be taken into account that linear extrapolation to high temperatures is only a rough approximation, since at low temperatures the temperature dependence of $D$ may be upward curved due to quantum effects (see e.g. in Ref. [43]). The interval of hydrogen diffusion coefficients reported in Refs. [44,45] for α phase ($Mg_2NiH_x$; $x = 0$–$0.3$) is slightly higher.

The present results are much lower than hydrogen diffusivities in pure Mg measured in Ref. [46] by the method of layer growth, calculated *ab initio* in Ref. [47] and obtained by gas permeation in Ref. [48]. They are also lower than values for a series of pure close-packed (hcp, fcc) metals reviewed in Ref. [43]. This can be explained by a commonly accepted fact that the rate of diffusion in hydride is generally lower than that in the matrix free of hydride [4].

It can be excluded that the low values of hydrogen diffusion coefficients obtained in the present paper were caused by difficult hydrogen diffusion in Mg oxide layer [49], which might be expected on the surface of particles, since no oxygen was found by SEM and no peaks of oxide were indicated in XRD spectra.

It is obvious from Table 1 that the obtained values of $\tau_{0i}$ decrease with the increasing desorption temperature $T_d$, which

Table 2
Arrhenius parameters of effective hydrogen diffusion in heterogeneous matrices with predominance of high-temperature β-phase $Mg_2NiH_4$ (HT), low-temperature un-twinned β-phase (LT1) and low-temperature twinned β-phase (LT2), respectively

| Matrix | $Q$ (kJ/mol) | ln $D_0$ ($D_0$ in m$^2$/s) |
|---|---|---|
| HT | $42.7 \pm 8.1$ | $-20.9 \pm 1.8$ |
| LT1 | $109 \pm 12$ | $-5.3 \pm 2.8$ |
| LT2 | | $-8.73 \pm 0.24$ |

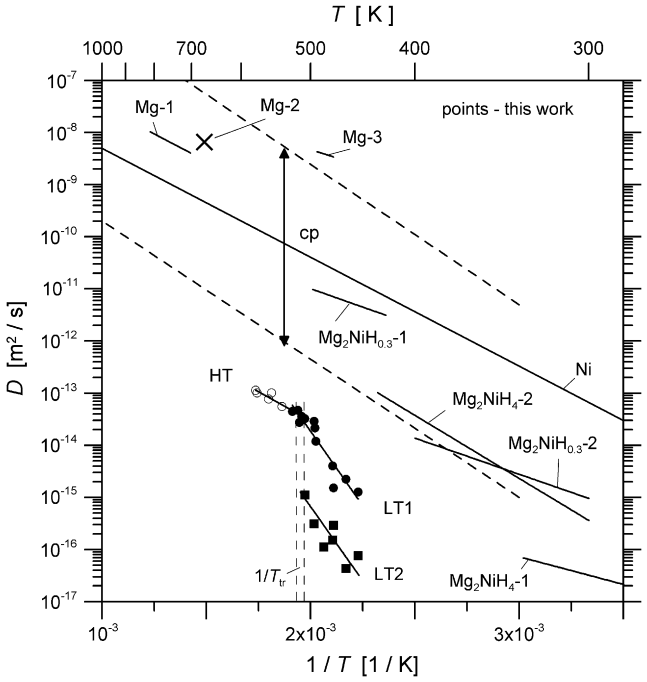


Fig. 10. Comparison of present results with literature data. $Mg_2NiH_4$-1 – [42], $Mg_2NiH_4$-2 – [37], $Mg_2NiH_{0.3}$-1 – [44], $Mg_2NiH_{0.3}$-2 – [45], Mg-1 – [46], Mg-2 – [47], Mg-3 – [48], Ni – [43], dashed lines – lower and upper limit of literature data on hydrogen diffusion coefficients in chosen close-packed (fcc, hcp) pure metals [43].

supports an expected fact that the desorption rate of hydrogen bound in hydride phase increases with increasing temperature.

## 4. Summary

In the present paper, the kinetics of hydrogen desorption from $Mg_2NiH_4$ intermetallic compound and relevant phase changes were studied. Two different techniques of intermetallic preparation were applied: (i) melting and casting and (ii) ball-milling and compacting the powder into pellets. Hydrogen charging of both materials followed in a pressure vessel under elevated pressure and temperature. The charging conditions for pellets were chosen in order to prepare (a) big or (b) small portion of LT2 phase. The hydrogen desorption was done far from the equilibrium, so that the driving force was high enough and the releasing of hydrogen was controlled by out-diffusion from the particles only. Conclusions of the present work can be summarized as follows.

1. Activation enthalpy $Q$ of hydrogen desorption above the transition temperature $T_{tr}$ is lower than $Q$ below the $T_{tr}$.
2. Two modes of desorption were observed below the $T_{tr}$, which are manifested by two distinct branches of desorption curve.
3. Presence of LT2 (twinned low-temperature $Mg_2NiH_4$ phase) causes very slow hydrogen desorption rate. It was observed that samples with initial excess of LT2 show very slow hydrogen desorption rate unless the amount of LT2 and LT1 phases becomes almost equal. Then, bustling hydrogen evolution occurs. This may be caused by different hydrogen diffusion trajectories in lattices LT1 and LT2. Such a phenomenon leading to different diffusivities of hydrogen in two polymorphs of manganite was reported in Ref. [50].
4. On the other hand, if the LT1 phase prevails over the LT2 at the start of the desorption, hydrogen evolves rapidly unless the amounts of LT1 and LT2 are roughly equilibrated. After that, the remaining hydrogen desorbs with dramatically slowed-down rate.
5. The findings sub 3 and 4 may be important for optimization of the structure of the material for hydrogen storage cells with rapid C/D characteristic: the presence of LT2 phase seems to be undesirable.
6. LT2 phase can be avoided, e.g. by the melting-and-casting technology and/or by charging at temperatures below the $T_{tr}$.

## Acknowledgements

This work was supported by the Czech Science Foundation under contract no. 106/07/0010 and by the Czech Academy of Sciences, project no. AV0Z20410507.

## References

[1] Trudeau ML. Advanced materials for energy storage. MRS Bull 1999;24:23.
[2] Ross DK. Vacuum 2006;80:1084.
[3] Bérubé V, Radtke G, Dresselhaus M, Chen G. Int J Energy Res 2007;31:637.
[4] Schwarz RB. In Ref. [1], p. 40.
[5] Massalski TB. Binary alloy phase diagrams. ASM International, ASM/NIST; 1996. CD ROM.
[6] Kusadome Y, Ikeda K, Nakamori Y, Orimo S, Horita Z. Scripta Mater 2007;57:751.
[7] Barkhordarian G, Klassen T, Borman R. Scripta Mater 2003;49:213.
[8] Blomqvist H, Rönnebro E, Noréus D, Kuji T. J Alloys Compd 2002;330–332:268.
[9] Kojima Y, Kawai Y, Haga T. J Alloys Compd 2006;424:294.
[10] Montone A, Antisari MV, Abazović N, Novaković JG, Pasquini L, Bonetti E, et al. Mater Sci Forum 2007;555:335.
[11] Gao RG, Tu JP, Wang XL, Zhang XB, Chen CP. J Alloys Compd 2003;356:649.
[12] Martin M, Gomel C, Borkhart C, Fromm E. J Alloys Compd 1996;238:193.
[13] Fernández GE, Rodríguez D, Mayer G. Int J Hydrogen Energy 1998;23:1193.
[14] Fang S, Zhou Z, Zhang J, Yao M, Feng F, Northwood DO. J Alloys Compd 1999;293:10.
[15] Liang G, Huot J, Boily S, Schulz R. J Alloys Compd 2000;305:239.
[16] Fernandez JF, Sanchez CR. J Alloys Compd 2002;340:189.
[17] Gabis IE, Voit AP, Evard EA, Zaika YuV, Chernov IA, Yartis VA. J Alloys Compd 2005;404:312.
[18] Li Q, Lin Q, Chou KCh, Jiang L. J Mater Sci 2004;39:61.
[19] Chou KCh, Xu K. Intermetallics 2007;15:767.
[20] Chou KCh, Li Q, Lin Q, Jiang LJ, Xu KD. Int J Hydrogen Energy 2005;30:301.
[21] Rudman PS. J Appl Phys 1979;50:7195.
[22] Gavra Z, Mintz MH. Inorg Chem 1979;18:3595.

[23] Hayakawa H, Ishido Y, Nomura K, Uruno H, Ono S. J Less-Common Met 1984;103:277.
[24] Noréus D, Kihlborg L. J Less-Common Met 1986;123:233.
[25] Zolliker P, Yvon K, Bearlocher Ch. J Less-Common Met 1986;115:65.
[26] Post LM, Murray JJ. J Less-Common Met 1987;134:15.
[27] Selvam P, Viswanathan B, Swamy CS, Srinivasan V. Int J Hydrogen Energy 1988;13:749.
[28] Hayashi S, Hayamizu K. J Less-Common Met 1989;155:31.
[29] Darnaudery JP, Pezat M, Darriet B, Hagenmuller P. Mater Res Bull 1981;16:1237.
[30] Blomqvist H, Noréus D. J Appl Phys 2002;91:5141.
[31] Blomqvist H, Noréus D, Babushkin O, Nion F, Vourien E. J Mater Sci Lett 2003;22:1487.
[32] Kim WG, Ur SC, Lee YG, Kim YJ, Hong TW. Mater Sci Forum 2007;544:311.
[33] García GN, Abriata JP, Sofo JO. Phys Rev B 1999;59:11746.
[34] ICSD Inorganic Crystals Structure Database, release 2007/1. Hermann-von-Helmholtz-Platz 1, Eggenstein-Leopoldshafen. Germany: FIZ Karlsruhe.
[35] JCPDS PDF-4 Full File 2004 Database. Newton Square, Pennsylvania, U.S.A.: ICDD.
[36] X'Pert HighScore Plus 2.0a. Almelo, The Netherlands: PANanalytical B.V.
[37] Senegas J, Mikou A, Pezat M, Dariet B. J Solid State Chem 1984;52:1.
[38] Sandrock GD, Suda S, Schlapbach L. In: Schlapbach L, editor. Hydrogen in intermetallic compounds, vol. II. Berlin: Springer; 1992 [chapter 5].
[39] Carslaw HS, Jaeger JC. Conduction of heat in solids. Oxford: Clarendon Press; 1959. p. 130, 184, 240.
[40] Crank J. Mathematics of diffusion. Oxford: Clarendon Press; 1957. p. 88.
[41] Borg RJ, Dienes GJ. An introduction to solid state diffusion. London: Academic Press Inc.; 1988. p. 225.
[42] Senegas J, Song MY, Pezat M, Darriet B. J Less-Common Met 1987;129:317.
[43] Wipf H. Hydrogen in metals III. In: Wipf H, editor. Topics in applied physics. Berlin, Heidelberg, New York: Springer; 1997. p. 51.
[44] Toepler H, Buchner H, Saeufferer K, Knorr K, Prandl W. J Less-Common Met 1982;88:397.
[45] Hayashi S, Hayamizu K, Yamamoto O. J Phys Chem Solids 1984;45:555.
[46] Renner J, Grabke HJ. Z Metallkde 1978;69:639.
[47] Schimmel HG, Kearley GJ, Huot J, Mulder FM. J Alloys Compd 2005;404:235.
[48] Nishimura C, Komaki M, Amano M. J Alloys Compd 1999;293:329.
[49] Monge MA, Gonzales R, Popov AI, Pareja R, Chen Y, Kotomin EA, et al. Defect Diffus Forum 1999;169–170:1.
[50] Balachandran D, Morgan D, Ceder G. J Solid State Chem 2002;166:91.